



Contents lists available at ScienceDirect

Journal of King Saud University – Science

journal homepage: [www.sciencedirect.com](http://www.sciencedirect.com)

Original article

# Surface functionalization of highly luminescent carbon nanodots from *Dioscorea hispida* with polyethylene glycol and branched polyethyleneimine and their *in vitro* study

Regina Sisika A. Sonthanasamy<sup>a</sup>, Shazrul Fazry<sup>b</sup>, Bohari M. Yamin<sup>a</sup>, Azwan Mat Lazim<sup>a,\*</sup><sup>a</sup>School of Chemical Sciences and Food Technology, Faculty of Science and Technology, Universiti Kebangsaan Malaysia, 43600 Bangi, Selangor, Malaysia<sup>b</sup>School of Bioscience and Biotechnology, Faculty of Science and Technology, Universiti Kebangsaan Malaysia, 43600 Bangi, Selangor, Malaysia

## ARTICLE INFO

## Article history:

Received 26 July 2017

Accepted 5 May 2018

Available online 9 May 2018

## Keywords:

C-dots

Gadong starch

BPEI

PEG<sub>1500N</sub>

Nanoparticles

Luminescence

## ABSTRACT

Synthesized carbon dots (C-dots) from *Dioscorea hispida* (Gadong tuber) starch were modified with passivating agents such as *O,O*-bis(3-aminopropyl)polyethylene glycol 1500 (PEG<sub>1500N</sub>) and branched polyethyleneimine (BPEI) to increase the functional efficiency of C-dots to be used in biological investigations. After surface modification, the C-dots decreased in size from 6–25 to 3–20 nm without changing their morphology. The modified C-dots were fluorescent, and the fluorescence peak gradually shifted to a longer excitation wavelength (from 420 to 500). Upon modification, thereby elucidating a competitive quantum yield of 15% (C-dots-PEG<sub>1500N</sub>) and 12.6% (C-dots-BPEI). The UV-visible spectrum of the C-dots modified with PEG<sub>1500N</sub> contained an absorption peak at 290 nm, whereas, that of the C-dots modified with BPEI contained peak at 360. Fourier-transform infrared analysis showed a peak at 1700 cm<sup>-1</sup> (C-dots-PEG<sub>1500N</sub>) and 1697 cm<sup>-1</sup> (C-dots-BPEI) that corresponds to the amide (–HCONH–) carbonyl bond, indicating that PEG<sub>1500N</sub> and BPEI had been successfully passivated on the surface of C-dots. To examine photothermal response, irradiation was carried out for 5 min using three different instruments which is UV-lamp (365 nm), visible lamp and laser (532 nm, 1 W/cm<sup>2</sup>) where temperature for each sample increased respectively. C-dots demonstrated not losing their luminescent properties upon irradiation to UV-lamp and laser for 30 min. Contrary, the intensity of fluorescence reduced when it exposed to the visible lamp for the same period. *In vitro* studies of the modified C-dots with zebrafish (*Danio rerio*) revealed that C-dots-PEG<sub>1500N</sub> is non-toxic while C-dots-BPEI is highly toxic to the fish embryos. Significantly, this study has successfully demonstrated that Gadong tuber starch can be used as a starch-based modifier for C-dots; which possibly can be utilized as a nanocarrier with thermal sensing properties.

© 2018 The Authors. Production and hosting by Elsevier B.V. on behalf of King Saud University. This is an open access article under the CC BY-NC-ND license (<http://creativecommons.org/licenses/by-nc-nd/4.0/>).

## 1. Introduction

Nanotechnology concerns materials measuring in size range of one to hundreds of nanometres. Nanomaterials play an important role in biomedicine, particularly in the areas of drug and gene therapy, as diagnostic probes, and biosensing. This is due to their biocompatibility, low cytotoxicity, and ability to cross the cell

membrane (Bianco et al., 2005; Dumortier et al., 2006; Pantarotto et al., 2004a; Kam et al., 2004). Increasingly, the development of nanostructured materials is receiving interest for its applications in gene therapy, for example, gene transfer or gene delivery.

Through chemical modification, inorganic nanoparticles such as gold nanoparticles, silica nanoparticles, semiconductor quantum dots, carbon nanotubes, nano diamonds, and graphene have been explored as non-viral tools for nucleic acid delivery (Veisoh et al., 2011; Namgung et al., 2010; Radu et al., 2004; He et al., 2011; Lee et al., 2010; Zhang and Liu, 2010; Bardi et al., 2010; Pantarotto et al., 2004b; Liu et al., 2011; Zhang et al., 2011; Kim et al., 2011; Baker and Baker, 2010; Hardman, 2006). Among this group of nanoparticles, recently, fluorescent carbon dots (C-dots) have drawn tremendous attention in many applications include gene therapy. C-dots belong to a new class of carbon-based nanomaterials that can be synthesized from natural materials. In

\* Corresponding author.

E-mail addresses: [shazrul@ukm.edu.my](mailto:shazrul@ukm.edu.my) (S. Fazry), [bohari@ukm.edu.my](mailto:bohari@ukm.edu.my) (B.M. Yamin), [azwanlazim@ukm.edu.my](mailto:azwanlazim@ukm.edu.my) (A.M. Lazim).

Peer review under responsibility of King Saud University.

<https://doi.org/10.1016/j.jksus.2018.05.004>

1018-3647/© 2018 The Authors. Production and hosting by Elsevier B.V. on behalf of King Saud University.

This is an open access article under the CC BY-NC-ND license (<http://creativecommons.org/licenses/by-nc-nd/4.0/>).

addition, they are fluorescent. Compared to the more traditional semiconductor quantum dots and organic dyes, photoluminescent C-dots are superior, having a high aqueous dispersity, robust chemical inertness, easy functionalization, high resistance to photobleaching, low toxicity, and excellent biocompatibility (Wang and Hu, 2014; Lim et al., 2015; Li et al., 2012). Therefore, aside from gene delivery, much attention has also been paid to their potential applications in biological labelling, bioimaging, and drug delivery (Sachdev and Gopinath, 2015; Zhang and Yu, 2016). Many research groups have reported that C-dots been used for biomarker, metal ions sensing, as a nanocarrier, and drug delivery vehicles (Li et al., 2012; Thakur et al., 2014; Qin et al., 2013; Huang et al., 2014; Borse et al., 2017; Thakur et al., 2016). C-dots have been utilized as dual sensing material based on their excellent fluorescence properties together with intracellular sensing (Borse et al., 2017). Besides, C-dots have been explored as a theragnostic agent with triplet functions as drug carrier, bioimaging and heightened antimicrobial activity (Thakur et al., 2014).

Currently, many reports have shown the advantage of surface modification of C-dots concerning their applications in many fields. The C-dots surfaces were also modified through passivation with polycations to enhance the solubility and quantum yield of C-dots. Branched polyethyleneimine (BPEI) and diamine-terminated oligomeric poly (ethylene glycol) (PEG<sub>1500N</sub>) are among the most effective cationic polymers studied to date (Behnam et al., 2013). Both polymers are highly efficient passivating agents which enhanced surface energy stabilization, give high impact to the fluorescence emissive properties and have low toxicity (Liu et al., 2012; Wu et al., 2013). Additions of polycations to the carbon surface exhibit strong photoluminescence because of the introduction of nitrogen atoms that originate from the polycations (Sun et al., 2006; Peng and Travas-Sejdic, 2009). Surface passivation of C-dots by PEG<sub>1500N</sub> are stable towards photobleaching and stable in water for more than half a year (Mao et al., 2010). Addition of BPEI and PEG<sub>1500N</sub> prevent C-dots from affecting by quench reagents and environmental factors. Polycations acts as a polymer shield onto the passivated C-dots can prevent C-dots from fluorescence-quenching of external factors (Mao et al., 2010). Consequently, BPEI and PEG<sub>1500N</sub> have been used as surface-modifying agents to increase the performance of C-dots by enhancing their fluorescence properties and ability as a nanocarrier (Borse et al., 2017; Wu et al., 2013; Mao et al., 2010; Liu et al., 2012).

Previous studies have used poly(propionylethylenimine-co-ethylenimine) (PPEI-EI) and PEG<sub>1500N</sub> as a modifying agent in bioimaging (Sun et al., 2006; Cao et al., 2007; Yang et al., 2009). However, there are few researches on fabrication of C-dots using natural plant materials as carbon source and also few studies related to the modification of starch-based surface deposits in biomedical and bioimaging subjects. This is due to the difficulty in finding suitably modified C-dots for targeting cells and producing an adequate response signal (Dong et al., 2012). Nevertheless, the surface modification of carbon-based nanomaterials for gene delivery has been studied (Behnam et al., 2013; Liu et al., 2012). Many studies reported that these carbon-based nanomaterials have consisted varieties of chemical compounds including polyethyleneimine (PEI) and nanotube carbons (Behnam et al., 2013; Zhou et al., 2007; Xu et al., 2004). PEI, for example has been used to prepare and modify carbon nanoparticles. It is also highly potential to be used as proton sensor for monitoring metabolic processes that are accompanied by proton release. Carbon nanoparticles prepared and modified with BPEI showed low cytotoxicity and favourable biocompatibility (Shen et al., 2013). Furthermore, research concerning PEG-functionalized C-dots in mice has shown that C-dots are non-toxic, suggesting that they may be biocompatible *in vivo* with possible applications in optical imaging and relevant to biomedical applications (Yang et al., 2009).

Apart from the recent modification of C-dots nanomaterials with chemical compounds, current research on fluorescent carbon nanomaterial has been focused on their theranostics properties which showed further surface modification was not a necessary to be used and performed as a multifunctional purpose. This is due to their combined functionality of photothermal and photodynamic which have affected on the biomedical field. As an example, synthesized graphene quantum dots (GQDs) and C-dots from natural plant have demonstrated excellent photothermal, photodynamic properties and also highly therapeutic activity in cancer cells studies (Thakur et al., 2017; Lee et al., 2016). Furthermore, GQDs have also been used as a temperature sensing probes due to their thermal sensing ability in biomedical nanotechnology (Kumawat et al., 2016). Despite of their vital performance, there is only few studies about photothermal effects on fluorescent carbon nanomaterial. Photothermal or thermal has become important subject of studies because it helps to minimizes damage to normal tissues (Liu et al., 2015; Huang et al., 2013; Cheng et al., 2012; Yang et al., 2010). Therefore, photothermal properties of a carbon-based nanomaterial is an important factor to be contemplated in terms of reducing the risk of normal cells to be damaged in biomedical applications.

Previously, C-dots were successfully synthesized from natural materials by a simple synthetic route from a low-cost precursor, i.e., Gadong starch (Sonthanasamy et al., 2015). These C-dots showed stable photoluminescence, high biocompatibility, high cost-effectiveness, excellent fluorescence, excellent water dispersity, and high sensitivity. C-dots from Gadong starch are naturally photoluminescent, which means that they do not require any passivating agents to show luminescence property. Therefore, starch based C-dots were used in this study to investigate ways to increase their utilization in the biological field. This study describes the modification of the surface of C-dots prepared from Gadong starch with BPEI and PEG<sub>1500N</sub> to increase the functionality of C-dots. The modified C-dots were investigated in terms of their fluorescence, toxicity and photothermal effects with respect to their use in gene therapy. Transmission electron microscopy (TEM) and high-resolution transmission electron microscopy (HR-TEM) was used to observe the C-dots morphology, and Fourier-transform infrared (FTIR), UV-vis, and fluorescence measurements were conducted to analyse the C-dots fluorescence performance. Further investigation was carried out to determine the toxicity of the modified C-dots to ensure their safety as nano carriers. The cationic polymer-modified C-dots were tested *in vitro* on 1-h post-fertilization (hpf) zebrafish (*Danio rerio*) embryos.

## 2. Materials and method

### 2.1. Materials

All chemicals were of reagent grade and used without further purification. BPEI, PEG<sub>1500N</sub>, and quinine sulfate were purchased from Sigma-Aldrich (USA & UK). Ultrapure water (~18.2 MΩ·cm, 25 °C) was obtained from a water purifying system (Sartorius, Model Arium®611DI). Embryos were obtained from the Department of Biochemistry, Faculty of Biotechnology and Biomolecular Sciences, Universiti Putra Malaysia.

### 2.2. Modification of the carbon nanodots

Starch nanoparticles were prepared from Gadong tubers using the method described by Kim et al. (2012). The starch nanoparticles were converted to C-dots following the method of Chin et al. (2012). The synthesized C-dots were modified according to the method outlined by Mao et al. (2010). Approximately 0.2 g of O; O-bis(3-aminopropyl)polyethylene glycol 1500 (PEG<sub>1500N</sub>) was

mixed with 50 mL of a C-dot solution (0.5 mg/mL), and the mixture was heated to 120 °C for 72 h under nitrogen flow. After the reaction, the PEG<sub>1500N</sub>-passivated C-dots were cooled to room temperature followed by dialysis (cutoff molecular weight 8000–14,000) and ultrafiltration (cutoff = 30 kDa). The same procedure was used to modify the C-dots with BPEI.

### 2.3. Morphology and average particle size

The morphology and particle size of the C-dots and surface-passivated C-dots were analyzed using a high-resolution transmission electron microscope (HR-TEM) (JEOL, JEM-200F) with accelerating voltage 200 kV, and a transmission electron microscopy (TEM) (Philips) operated at 300 kV. A drop of the C-dots suspension was deposited on a carbon-coated microscopy grid and dried at room temperature. The modified C-dots average particle sizes were determined using the IMAGE-J and iTEM programs (Borse et al., 2017; Mao et al., 2010).

### 2.4. Particle size distribution and zeta potential analysis

The particle size distribution and zeta potential of both the C-dots and modified C-dots were determined using Dynamic Light Scattering (DLS) and Zeta analyzer (Malver Instrument Ltd.). The diluted aqueous C-dots solutions were sonicated for 15 min before analysis. The experiment was carried out three times to validate the data.

### 2.5. UV-visible absorbance measurements

UV-vis absorbance measurements of the sample were obtained using a UV-vis spectrophotometer (UV-2450 SHIMADZU). The suspension was diluted with ultra-pure water in a ratio of 1:2 (mL) and its absorbance was monitored between 200 and 800 nm (Mao et al., 2010). Ultrapure water was used as a reference.

### 2.6. Fluorescence of the modified C-dots

Fluorescence emission spectra were recorded using Perkin Elmer LS 55-Luminescence Spectrophotometer using path length of 1 cm slit width relative to excitation and emission were both 2.5 nm. The suspension was diluted with ultrapure water in a ratio of 1:2 (mL) and scanned from 450 to 800 nm, while excitation was tested from 200 to 500 nm (Mao et al., 2010). Gadong starch was used as a control.

### 2.7. Fourier transform infra-red spectroscopy

Fourier transform infra-red (FTIR) spectroscopy was performed to analyze the functional groups present on the surface of modified C-dots. The modified C-dots were prepared in a sodium chloride pellet, and the spectra were collected between 400 and 4000 cm<sup>-1</sup>.

### 2.8. Ultraviolet lamp (UV-lamp)

The fluorescence properties of the modified C-dots were further confirmed using a UV-lamp. The modified C-dots were observed under the blue-light excitation at a wavelength of 365 nm.

### 2.9. Quantum yield measurements

The quantum yield (QY) of the modified C-dots was determined by a comparative method (Mendes et al., 2017). Quinine sulfate in 0.1 M H<sub>2</sub>SO<sub>4</sub> (literature  $\phi = 54\%$ ) was selected as a standard to calculate the QY of the test samples (i.e. modified C-dots) was dissolved in ultrapure water at different concentration (Wu et al., 2013). All the absorbance values of the solutions at the excitation

wavelength were measured with UV-vis spectrophotometer. Photoluminescence (PL) emission spectra of all the sample solutions were recorded by Perkin Elmer LS 55- Luminescence Spectrophotometer at an excitation wavelength of 350 nm (Quinine sulfate). The integrated fluorescence intensity is the area under the PL curve in the wavelength range from 380 to 600 nm. A graph, was then plotted using the integrated fluorescence intensity against the absorbance and a trend line was added for each curve with intercept at zero. Absolute values were calculated according to the following equation (Zhu et al., 2015):

$$\phi_x = \phi_{st} \left( \frac{\text{Grad}_x}{\text{Grad}_{st}} \right) \left( \frac{\eta_x}{\eta_{st}} \right) \quad (1)$$

where  $\phi$  is QY, subscripts  $x$  and  $st$  represents test and standard respectively,  $Grad$  is the slope of fluorescence intensity versus absorbance plot,  $\eta$  is the refractive index of the solvent ( $\eta = 1.33$  for water, and sulfuric acid).

### 2.10. Photothermal performance of C-dots

The photothermal effect of the C-dots and modified C-dots was determined by using methods as previously reported (Lee et al., 2016) with slightly modifications. C-dots and modified C-dots (C-dots-PEG<sub>1500N</sub> and C-dots-BPEI) were dissolved in Phosphate buffered saline (PBS) at different concentrations (0 mg/mL to 20 mg/mL) separately. Each C-dots solution (1 mL) was introduced in a quartz cuvette and irradiated with UV-lamp (365 nm), visible light (LED spotlight) and 532 nm- laser light (Mendes et al., 2017) at a power density of 1 W/cm<sup>2</sup> for 5 min. To observe the photothermal characteristics of C-dots and modified C-dots solutions, a thermometer was inserted into the cuvette to contact the C-dots solutions, and the temperature was recorded every 1 min. PBS (0  $\mu$ g/mL) was used as a control.

### 2.11. Fish embryo toxicity (FET) tests

E3 embryo media (5.03 m M NaCl, 0.17 m M KCl, 0.33 m M CaCl<sub>2</sub>·2H<sub>2</sub>O, 0.33 m M MgSO<sub>4</sub>·2H<sub>2</sub>O and 0.1% (w/v) methylene blue) were used to wash and maintain viable fertilised eggs at room temperature at all times. In a 96-well plate, the embryos were placed in single wells 1 hpf and were maintained in 180  $\mu$ L of E3 embryo medium at room temperature. The toxicity effects of C-dots, C-dots-BPEI, and C-dots-PEG<sub>1500N</sub> on the development of *Danio rerio* embryo were evaluated by exposing fertilised eggs to 0.5 mg/mL concentration of unmodified and modified C-dots respectively and three replicates, ( $n = 3$ ) were set for each of the test. In this study, embryos from the three early embryonic development stages (24 hpf, 48 hpf, and 72 hpf) were sampled and analysed. These FET tests were carried out in accordance with the OECD draft guidelines (OECD, 2006, 2013).

## 3. Results and discussion

### 3.1. Morphology and average particle size

The C-dots synthesis was performed by a chemical ablation method by dehydrating starch nanoparticles with concentrated H<sub>2</sub>SO<sub>4</sub> followed by breaking the carbonaceous particles into individual C-dots with HNO<sub>3</sub> and finally, passivated with passivating agents such as PEG<sub>1500N</sub> and BPEI. The morphological characteristics of synthesized and surface passivated C-dots were observed by TEM and HR-TEM. Fig. 1(a–c) shows the TEM and HR-TEM image of modified and unmodified C-dots. A congruent round shape was obtained for all C-dots samples and the C-dots ranged in size from 6 to 25 nm (C-dots), 3 to 12 nm (C-dots-PEG<sub>1500N</sub>), and 4 to 20 nm

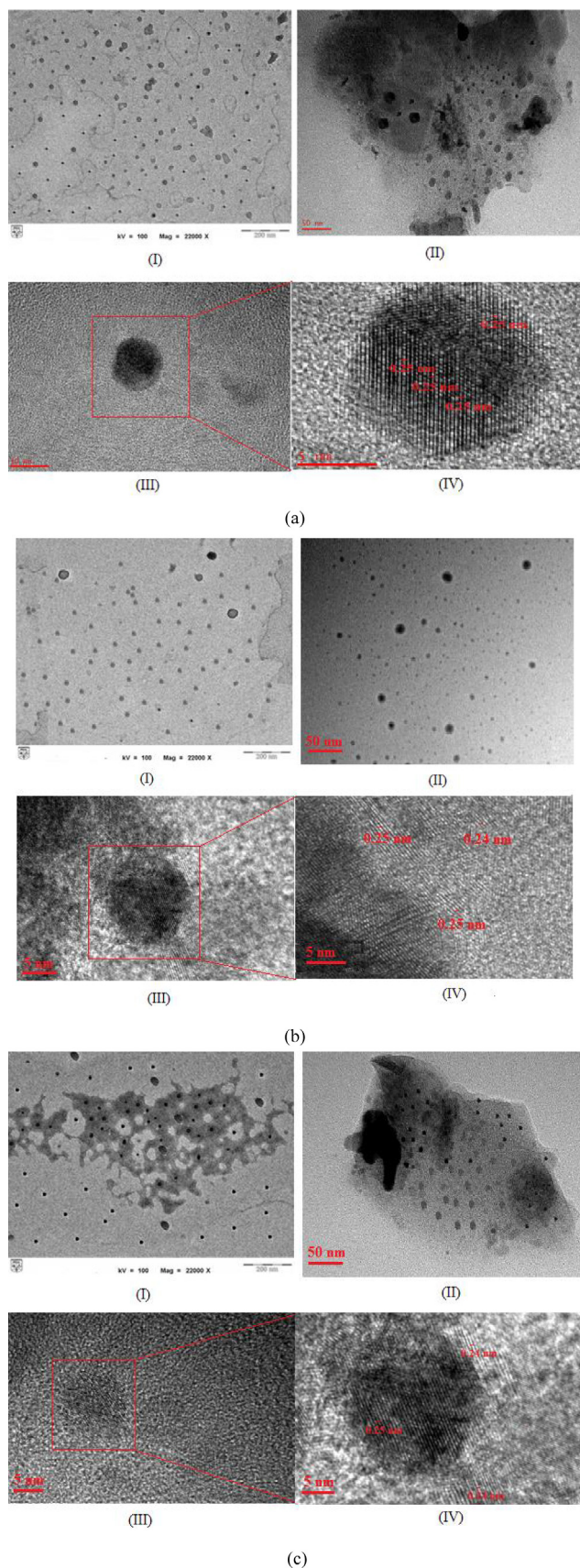


**Fig. 1.** Morphology image of (I) TEM, (II) HR-TEM, and (III) Lattice space of (a) carbon nanodots (C-dots) (b) surface modified C-dots with PEG<sub>1500N</sub> (c) surface modified C-dots with BPEI.

(C-dots-BPEI). Further heating has reduced the size of particles without changing the shape. The size distribution of the unmodified and modified C-dots was further verified by dynamic light scattering (DLS) analysis and shown in Fig. S1 (Supporting Information). The average size of C-dots and modified C-dots was measured to about  $24 \pm 4$  nm (C-dots),  $4.7 \pm 1.3$  nm (C-dots-PEG<sub>1500N</sub>), and  $6 \pm 0.8$  nm (C-dots-BPEI). Crystalline structure of C-dots was confirmed by HR-TEM analysis (figure a-IV). C-dots exhibited lattice spacing of 0.25 nm attributed to (002) facet of graphite indicating that the synthesized C-dots are graphitic in nature.

However, the synthesis of the C-dots resulted in particles with a variety of sizes. Therefore, for efficient applications of C-dots, complex separation methods including dialysis, chromatography, electrophoresis and sucrose density gradient centrifugation became mandatory to obtain uniformly sized C-dots (Li et al., 2012; Oza et al., 2015; Pandey et al., 2013). This step is necessary to determine the fluorescence properties of C-dots appropriately and for their use in the bioimaging and biomedical fields.

The shape and size of particles are concern in the biomedical applications. Most of the synthesized C-dots show spherical or round shape with size diameter below than 10 nm (Qin et al., 2013; Borse et al., 2017; Xu et al., 2013; Sha et al., 2013; Mehta et al., 2014; Li et al., 2014; Amjadi et al., 2014). Recently, a new and unique shape of C-dots called clathrates-like nanostructure was found and it was used as a nanocarrier. The clathrates-like morphology of C-dots was found to be extremely effective for the rapid release of drug and therefore it was labelled as a powerful drug vehicle (Pandey et al., 2017). The smallest size which is below 10 nm is preferable and it will easily penetrate through the cell membrane. In addition, the shapes of particles also affect the biological responses, and spherical, discoidal, rod-like, or filamentous shape allow better cell penetration (Barua and Mitragotri, 2014).

### 3.2. Absorption analysis of the modified C-dots

Fig. 2 shows the absorption peaks of unmodified and modified C-dots with PEG<sub>1500N</sub> and BPEI aqueous solution. The unmodified C-dots exhibited an absorbance peak at 290 nm. The absorption of the C-dots is typically ascribed to the presence of  $n \rightarrow \pi^*$  electron transitions associated with the C=O functional group. The absorption peak of the PEG<sub>1500N</sub>-modified C-dots occurred at 290 nm, which is like that of the unmodified C-dots. This absorbance peak indicated that the C=O bond was not broken, but the PEG<sub>1500N</sub> was bonded to the C-dots by amide bonds formed by condensation (Bartelmess and Giordani, 2014).

The UV absorption spectrum of the C-dots with modified with BPEI contains absorption peaks at 360 nm. A similar observation was reported by Dong et al. (2012) who reported UV-vis absorption peaks at wavelengths of 360 and 240 nm, resulting from the  $\pi \rightarrow \pi^*$  transitions of C=C electrons (Liu et al., 2012; Shen et al., 2013).

The aqueous solution of C-dots appears dark yellow colour, which emits green fluorescence under UV-lamp (365 nm) as displayed in the Fig. 2. Surface modified C-dots with PEG<sub>1500N</sub> and BPEI shows blue and dark green luminescence under 365 nm UV-ray whereas, raw starch solution does not show fluorescence properties. Therefore, the luminescence shown by the modified C-dots is proposed to arise from both the C-dots and the modifying agents (PEG<sub>1500N</sub> and BPEI).

### 3.3. Bonding configurations of the functional groups in the modified C-dots

FTIR spectroscopy was used to obtain information on the bonding in the C-dots and the location of the hydrogen atoms within the

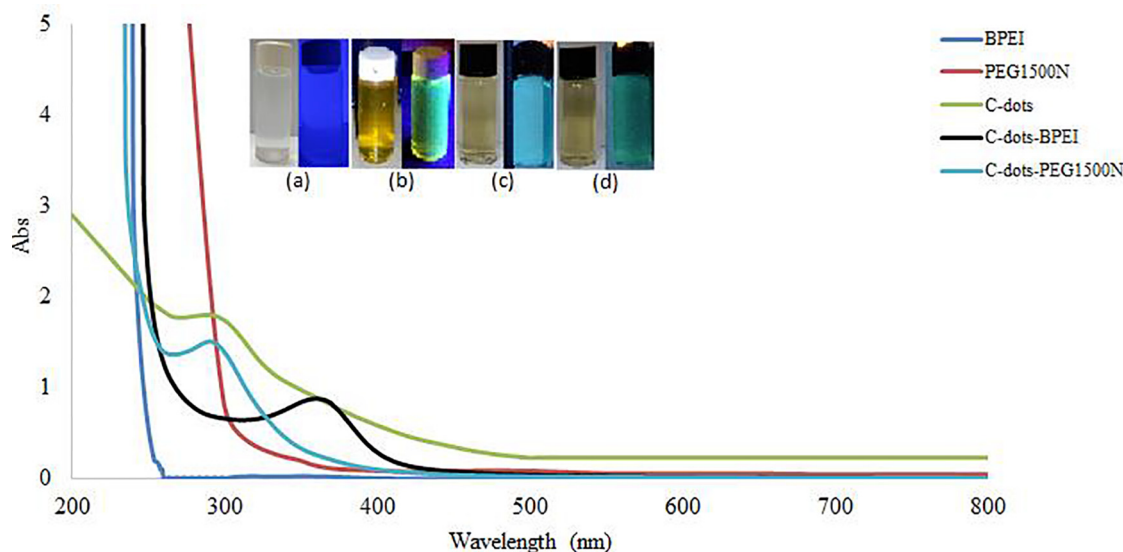


**Fig. 2.** UV absorbance spectrum of surface modified C-dots with PEG<sub>1500N</sub> and BPEI and aqueous solution of (a) starch (b) C-dots (c) C-dots-PEG<sub>1500N</sub> (d) C-dots-BPEI under UV-lamp.

particles. The FTIR spectra obtained for the unmodified C-dots and those modified with PEG<sub>1500N</sub> and BPEI (alongside the spectra of the modifying agents alone) are shown in Fig. 3a and b, respectively. Both modified C-dots spectra contain a broad absorption peak, followed by several overlapping peaks where most of the bands are due to the characteristic vibrations of the chromophores of different functional groups in the C-dots internal structure.

Most of the bands in the spectrum of the unmodified C-dots can be associated with the C–H and C=C bonds that are characteristic of organic compounds, and some of these bonds arise from the dehydration step (Galvez et al., 2002). The main band can be divided to four bands. The peak at 3433 cm<sup>-1</sup> corresponds to the stretching vibration of the O–H bond (Ray et al., 2009; Yan et al., 2014). The second band between 1500–2000 cm<sup>-1</sup> contains a peak at 1682 cm<sup>-1</sup>, arising from the stretching of the carbonyl group in the C-dots (Ray et al., 2009). The hydroxyl peak at 3433 cm<sup>-1</sup> reduces the intensity of the carbonyl absorption at 1682 cm<sup>-1</sup>. An absorption peak at 829 cm<sup>-1</sup> indicates that the starting material used is a polysaccharide. Absorption peaks at 2930, 1130, 1104, 997, 925 and, in particular, 832 cm<sup>-1</sup> (study 829 cm<sup>-1</sup>) in the FTIR spectrum are derived from the  $\alpha$ -glucose polysaccharides in the starting material (Prasad et al., 2011). Finally, an additional peak can be seen at 2092 cm<sup>-1</sup>, and this corresponds to C–H stretching, while that at 1456 cm<sup>-1</sup> is due to the bonds in the aliphatic CH<sub>3</sub> groups of the C-dots (Ray et al., 2009).

The main band from the PEG<sub>1500N</sub> spectrum Fig. 3a) can be divided to four groups. The peak at 3431 cm<sup>-1</sup> indicates NH stretching vibration (in the range of 3500–3000 cm<sup>-1</sup>, equivalent to stretching vibrations of OH groups or NH), whereas peaks at 2884, 2232, and 2157 cm<sup>-1</sup> suggest the presence of CH<sub>2</sub>, CH<sub>3</sub>, and CN groups (in the range of 3000–2000 cm<sup>-1</sup>) (Sachdev et al., 2013). Peaks at 1643, and 1573 cm<sup>-1</sup> indicated that CH, and NH groups are presented (in the range of 2000–1500 cm<sup>-1</sup>) (Sachdev et al., 2013), and vibrations at 1467, 1344, and 1279 cm<sup>-1</sup>, similar to those in the 3000–2000 cm<sup>-1</sup> range, revealed the presence of CH<sub>2</sub>, CH<sub>3</sub>, and CN groups (in the range of 1500–1000 cm<sup>-1</sup>) (Sachdev et al., 2013).

The absorption band at 3417 cm<sup>-1</sup> represents OH and NH groups, and the peaks arising from these vibrations overlapped each other. CH<sub>2</sub> and CH<sub>3</sub> stretching vibrations resulted in absorptions at 2920 and 2882 cm<sup>-1</sup>. A stretching vibration at 1700 cm<sup>-1</sup> corresponded to the amide I (–HCONH–) stretch, whereas the absorption peak at 1639 cm<sup>-1</sup> is possibly due to the conjugated

of CN bond, while the peak at 1575 cm<sup>-1</sup> corresponds to amide II (NH). The new absorption peak at 1700 cm<sup>-1</sup> confirmed that the surface of the C-dots had been successfully passivated with PEG<sub>1500N</sub>. Absorption peaks at 1469 and 1344 cm<sup>-1</sup> corresponded to –CH<sub>3</sub>. In addition, the sharp peak at 1280 cm<sup>-1</sup> is due to the amine I of CN bond. A peak at 1110 cm<sup>-1</sup> resulted from the symmetric vibrations of the –C–O–C– group (Sachdev et al., 2013).

Fig. 3b shows the BPEI spectrum, which is divided into two groups. The first group is in the range of 3500–2500 cm<sup>-1</sup>, which is equivalent to the stretching vibration of OH or NH. The peak at 3440 cm<sup>-1</sup> indicates an NH stretching vibration, whereas the absorption peaks at 2942 and 2868 cm<sup>-1</sup> are due to the presence of CH<sub>2</sub> groups. The second band lies within the range of 1500–1000 cm<sup>-1</sup>, where peaks at 1606, 1457, and 1307 cm<sup>-1</sup> indicate the presence of NH, CH<sub>2</sub> and CN (Liu et al., 2012).

As shown in Fig. 3b, the spectrum of the C-dots surface passivated with BPEI contains absorption bands that are characteristic of the NH groups in BPEI in the range of 3442 to 1304 cm<sup>-1</sup>, i.e., CH<sub>2</sub> at 2942, 2836, and 2100 cm<sup>-1</sup>, and CN at 1304 cm<sup>-1</sup>. Peak at 1590 cm<sup>-1</sup> which is caused by C=C stretching. This suggested BPEI was stable during the passivation of the C-dots. Furthermore, the sharp peak at 1700 cm<sup>-1</sup>, which is characteristic of an amide (–CONH–) group, suggested the BPEI was held on the surface of C-dots by amide bonds. The surface modification at a low temperature (<200 °C) allowed the complete carbonation without destroying the BPEI layers, as shown by FTIR. There are strong linkages (–CONH–) between the carbonyl groups of C-dots and NH<sub>2</sub> group of the BPEI, providing a stable coating (Liu et al., 2012).

Zeta potential analysis was conducted to determine the electrical charges of particles on the surface of an unmodified and a modified C-dots. Zeta potential of aqueous C-dots solution was found to be  $-32.2 \pm 11$  mV which shows the presence of negatively charged carbonyl functional group on the surface while the modified C-dots with PEG<sub>1500N</sub> and BPEI was found to be  $6.80 \pm 2.93$  mV and  $7.77 \pm 3.08$  mV, respectively (as shown in Fig. S2). The positive surface of modified C-dots is due the presence of positively charged amide functional groups, NH<sub>2</sub><sup>+</sup> on the surface from the passivating agents.

#### 3.4. Fluorescence properties of modified C-dots

The fluorescence spectra of PEG<sub>1500N</sub>, BPEI, starch, C-dots, C-dots-PEG<sub>1500N</sub>, C-dots-BPEI was recorded by changing the

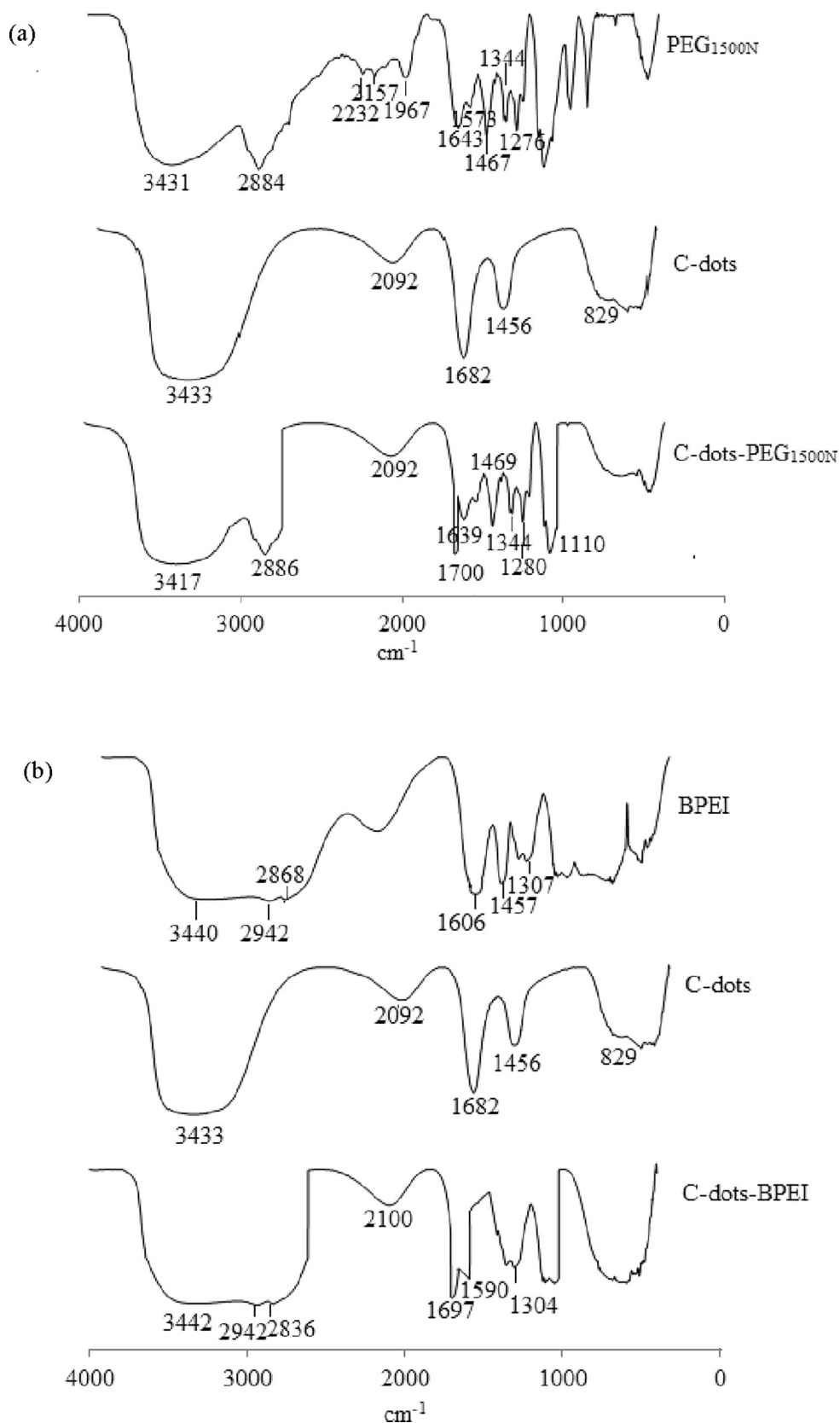
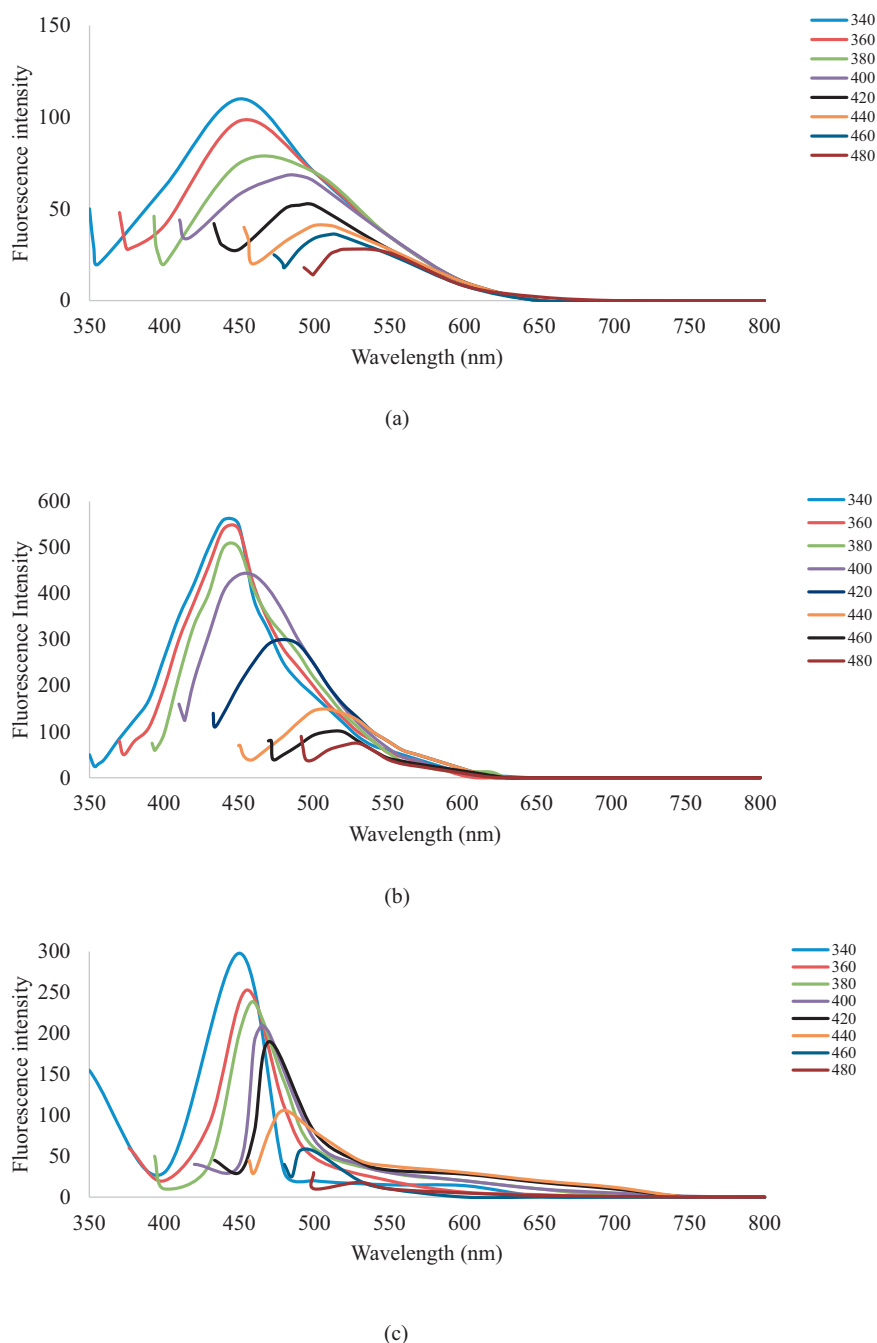


Fig. 3. FTIR Spectrum of modified C-dots with (a) PEG<sub>1500N</sub> (b) BPEI.

excitation wavelength. Fig. 4 shows the emission spectra of unmodified and modified C-dots, while the emission spectra of control materials such as PEG<sub>1500N</sub>, BPEI and starch were shown

in Fig. S3 of Supporting Information. The unmodified C-dots, which were synthesized from Gadong starch, naturally showed strong fluorescence. Therefore, the fluorescence of the modified



**Fig. 4.** The emission spectra of (a) unmodified C-dots; (b) PEG<sub>1500N</sub>-modified C-dots; and (c) BPEI-modified C-dots at different excitation wavelength.

C-dots can be compared to that of the unmodified C-dots based on their emission spectra.

The excitation wavelength when changes from 340 nm to 480 nm, the emission peak position of C-dots, C-dots-PEG<sub>1500N</sub>, C-dots-BPEI is red-shifted to longer wavelength from 350 nm to 500 nm and fluorescence intensity decreased remarkably, indicating a strong dependence on the excitation wavelengths. The fluorescence intensity of the modified C-dots is higher than the unmodified C-dots, indicating that the polycations had been successfully deposited on the surface of the C-dots.

Although until now the origins of fluorescence in C-dots are unclear, it is expected that this wavelength-dependent phenomenon comes from the different distribution of emissive energy traps on the surface of C-dots and the modified C-dots. As sug-

gested in the literature, the functional groups of precursors can be affected to the origin of the fluorescence emitted from C-dots (Liu et al., 2011; Zhao et al., 2008). A combination of amine and carboxyl groups in the compound resulting to enhance the most fluorescence activity of the modified C-dots (Baker and Baker, 2010; Hsu and Chang, 2012).

The fluorescent properties can be described by using quantum confinement theory, where the modifying agent traps the emission energy, thus exhibiting strong fluorescence, which has been previously observed in silicon nanocrystals (Mao et al., 2010). The establishment of strong bonds between the PEG<sub>1500N</sub> and BPEI with the C-dots trapped this energy, thus resulting in greater luminescence intensity compared to that of the unmodified C-dots. Functional groups such as carbonyl and amines were introduced to the surface

of modified C-dots, and these also entrap the excitation energy, resulting in greater photoluminescence (Zhou et al., 2012).

Based on photoluminescence properties, the quantum yield (QY) of modified C-dots with PEG<sub>1500N</sub> and BPEI was calculated by using quinine sulfate (excitation wavelength 350 nm) as a reference compound. Modified C-dots exhibited strong fluorescence with QY of C-dots-PEG<sub>1500N</sub> and C-dots-BPEI was found to be 15% and 12.6% respectively (as shown in Fig. S3), which was comparable to previously reported modified C-dots (Huang et al., 2014; Wu et al., 2013; Liu et al., 2012; Zhu et al., 2015; Mehta et al., 2014).

### 3.5. Photothermal effects of C-dots

The photothermal properties of C-dots and modified C-dots was examined using UV-lamp, visible lamp and 532 nm laser light (1 W/cm<sup>2</sup>) for 5 min. The temperature changes of C-dots and modified C-dots (Fig. S5 Supporting Information) at different

concentration (0.1–20 mg/mL) were measured and plotted in Fig. 5 (only certain significant concentrations of C-dots were shown while full result was reported in the Supporting Information section). In Photothermal study, the temperature increment was observed with increasing concentration of both C-dots. Modifying agents (PEG<sub>1500N</sub> and BPEI) on C-dots shows a slight impact on the temperature increment. Table 1 summarized the temperature rose for each sample when irradiated for 5 min by using UV-lamp, laser and visible lamp. The initial temperature recorded 27 °C (for UV-lamp and Visible lamp). Based on the observation made for each instrument, the modified C-dot gave better photothermal stability performance compared to the unmodified.

Using the similar method previously mentioned above, both samples (20 mg/mL) were further investigated to determine photo stability via their fluorescence properties (Figs. S6 and S7 Supporting Information). The intensity of the fluorescence increased upon exposure to the UV-lamp (365 nm) and laser (532 nm) for 15 min.

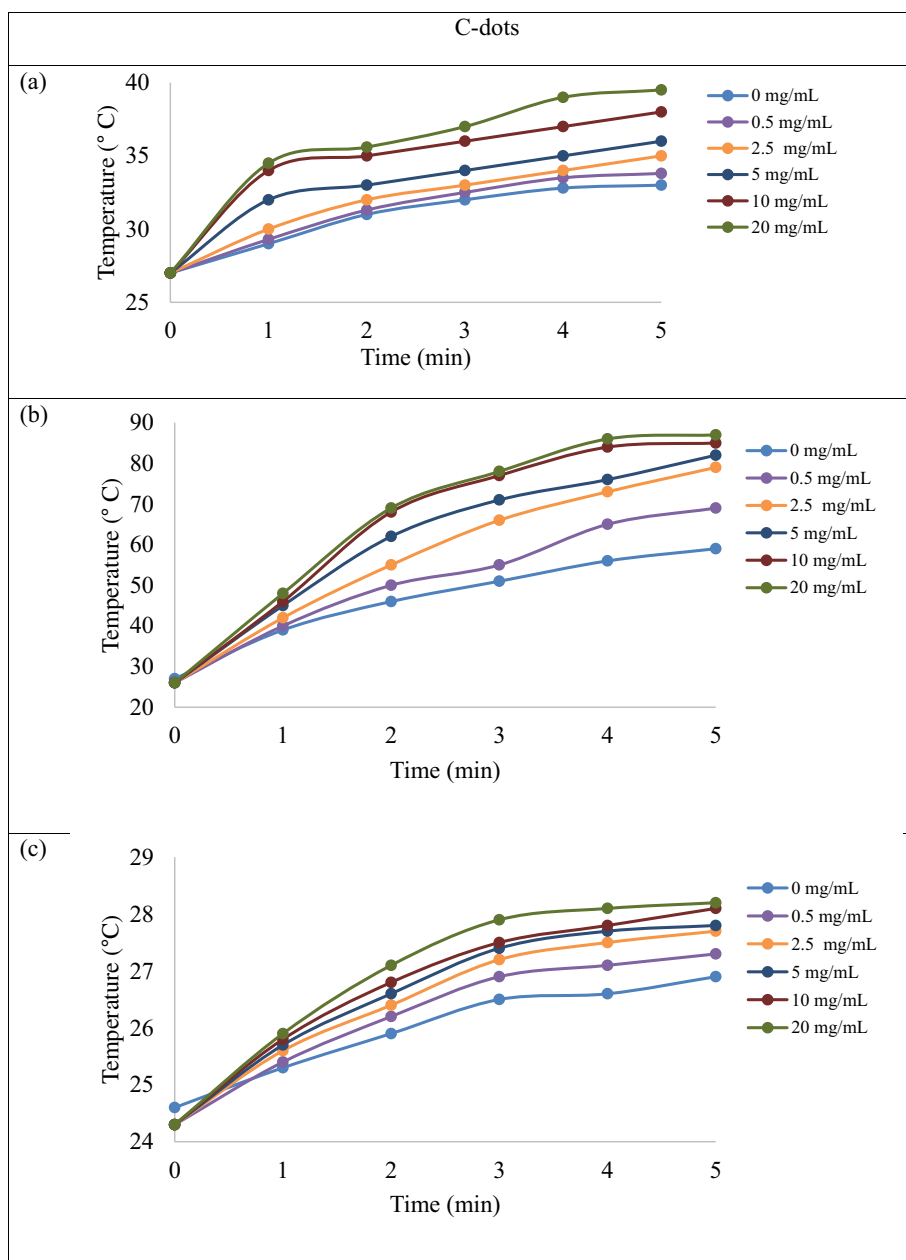


Fig. 5. Temperature increment of C-dots (0.1–20 mg/mL) after irradiation with UV-lamp (a), Visible lamp (b) and Laser (c) for 5 min.

**Table 1**  
Photothermal response of C-dots using three different irradiations medium.

Samples (concentration mg/ mL)	5 min of irradiation (°C)								
	C-dots			C-dots-PEG <sub>1500N</sub>			C-dots-BPEI		
	UV-lamp	Laser (532 nm)	Visible lamp	UV-lamp	Laser (532 nm)	Visible lamp	UV-lamp	Laser (532 nm)	Visible lamp
0	33.0	26.9	59.0	33.0	26.9	59.0	33.0	26.9	59.0
0.1	33.2	27.0	60.0	33.8	26.9	60.0	33.8	26.3	59.8
0.25	33.6	27.1	63.0	35.0	27.1	65.0	34.2	26.5	66.0
0.5	33.8	27.3	69.0	36.0	27.2	71.0	35.0	26.8	71.0
1.0	33.9	27.4	75.0	36.8	27.3	75.0	35.6	27.2	75.0
2.5	35.0	27.7	79.0	37.0	27.5	82.0	36.0	27.8	81.0
5.0	36.0	27.8	82.0	38.0	27.6	83.0	37.0	28.2	83.0
10.0	38.0	28.2	85.0	40.0	27.8	85.0	38.8	28.7	84.0
20.0	39.5	28.2	87.0	41.5	27.9	86.0	41.0	28.9	86.0

There were no changes to the results although extension was made up to 30 min. This was in agreement with observation reported by [Thakur et al. \(2017\)](#). In contrast, the fluorescence intensity of both samples decreased with the increasing of time exposure (from 15 to 30 min) to visible light irradiation.

Consequently, to the elevated changes of temperature [Table 1](#), the fluorescence intensity declined tremendous. Increasing in temperature is directly proportional to the energy transfer causes decreasing in collision time of the molecules, which is superior to an effectual collision quenching the fluorescence of the particle ([Papadopoulou et al., 2005](#); [Kuzkova et al., 2014](#)). [Kumawat et al. \(2016\)](#) also reported the fluorescence intensity decreased over temperature increment. For further application, by using variation temperature in cells as model, his group has successfully justified that QDs have the ability to detect the temperature changes occurred in the cellular environment. Researched by [Menter \(2006\)](#) were elegantly demonstrated that fluorescence was affected by proteins denaturation in cell due to the temperature changes. Due to that, the QDs can alternatively be used as temperature sensing probe. Likewise, C-dots also gave similar properties therefore, it was suggested to be used as a medium of thermal sensing in biomedical applications.

### 3.6. Fish embryo toxicity (FET) tests

C-dots were used to replace quantum dots (QD), which are composed of heavy metals. [Li et al. \(2012\)](#) reported that QDs are toxic both *in vivo* and *in vitro*. This makes QDs undesirable for biomedical and industrial applications because of the risk of health problems and aquatic and terrestrial pollution. C-dots, on the other hand, are viewed as a safer alternative to QDs ([Li et al., 2012](#)) because they can easily penetrate cells without disrupting the nuclei. Disruption of the nuclei would cause genetic instability, which is undesirable ([Li et al., 2012](#); [Jeong et al., 2009](#)).

[Fig. 6](#) shows the C-dots and modified C-dots were introduced into fish embryo to evaluate their toxicity capabilities using confocal microscopy test *in vitro*. Cell viability studies suggested C-dots exhibited cytotoxicity and posed no significant toxicity effect for the early 48 h. In the early stages, from 24 to 48 h, the fish embryos (70%) developed normally, whereas the embryos died after 72 h. The modified fluorescent C-dots with BPEI became toxic to the fish embryos after exposure for 24 h, as shown in [Fig. 6](#) while the modified C-dots with PEG<sub>1500N</sub> exhibited cytotoxicity and posed no significant toxicity effect. Within 72 h, fish embryos exposed with the C-dots-PEG<sub>1500N</sub> were observed to develop normally (100%) without any sign of lethality.

We selected zebrafish as model because it is a vertebrate organism and the embryos develop most of the major organ system present in mammals by less than a week ([Rubinstein, 2006](#)). Zebrafish

embryos also an important for studying toxicity, *in vivo* system damage, the transport and biocompatibility of nanoparticles, their small size, transparency and it is easy to observe the transport and the effects of nanoparticles in real-time and ability to absorb compounds through the water. Besides that, the period of embryo development can be controlled by regulating the light-dark cycle. Importantly, zebrafish are very homologous with mammals and approximately 70% of human gene are orthologous to those in zebrafish, so modelling human disease with zebrafish as model becomes an important and fast strategy to use as a model organism ([Howe et al., 2013](#); [Kettleborough et al., 2013](#)). Embryonic development is an important model for studying the toxicity and these possible risks posed to human health and the environment are proposed based on these developmental results. Therefore, zebrafish embryo is unique for these studies compared with other vertebrate model systems such as mice and rats ([Wang et al., 2010](#); [Kimmel et al., 1995](#)).

The C-dots modified with BPEI were more toxic, suggesting that C-dots modified with BPEI are not safe for biological or biomedical applications, and this result agrees with previous findings ([Moghimi and Andresen, 2009](#)). The cytotoxicity of the BPEI is due to its positive charge, which causes serious damage to the cell membrane.

In contrast, the C-dots modified with PEG<sub>1500N</sub> showed no significant toxic effects on the embryos. This is supported by a previous report that showed that PEG<sub>1500N</sub> is not toxic to cells ([Li et al., 2012](#)). Modified C-dots contain two fundamental spatial components which is the core and the corona that interact with the environment or solvent. The reduction of toxicity of C-dots-PEG<sub>1500N</sub> have been caused by reduced contact between the C-dots and embryos. PEGylation reduced the contact between the nanomaterials and cells ([Chen et al., 2015](#)).

The basic challenges of nanoparticles are include uptake by the reticuloendothelial system (RES), in which tiny particles are rapidly shuttled out of circulation to the liver, spleen or bone marrow and nonspecific binding of nanoparticles to non-targeted areas ([Joker et al., 2011](#)). Nanoparticles toxicity often arise due to this RES accumulation. Aggregation can lead to nanoparticles entrapment in the liver, lungs or elsewhere due to capillary occlusion ([Knop et al., 2006](#)). Therefore, addition of PEG to the C-dots surface can reduce many of these challenges. PEGylation has been widely used in nanomaterials because it can improve the biocompatibility and reduce the clearance by the reticuloendothelial ([Gao et al., 2013](#); [Gao et al., 2014](#)). Addition of PEG to C-dots reduces RES uptakes and increases circulation time versus uncoated counterparts. PEG decreases the amount of attraction between C-dots by increasing the steric distance between them and increasing hydrophilicity via ether repeats forming hydrogen bonds with solvent. Other benefits of PEGylation include modifying the size of the

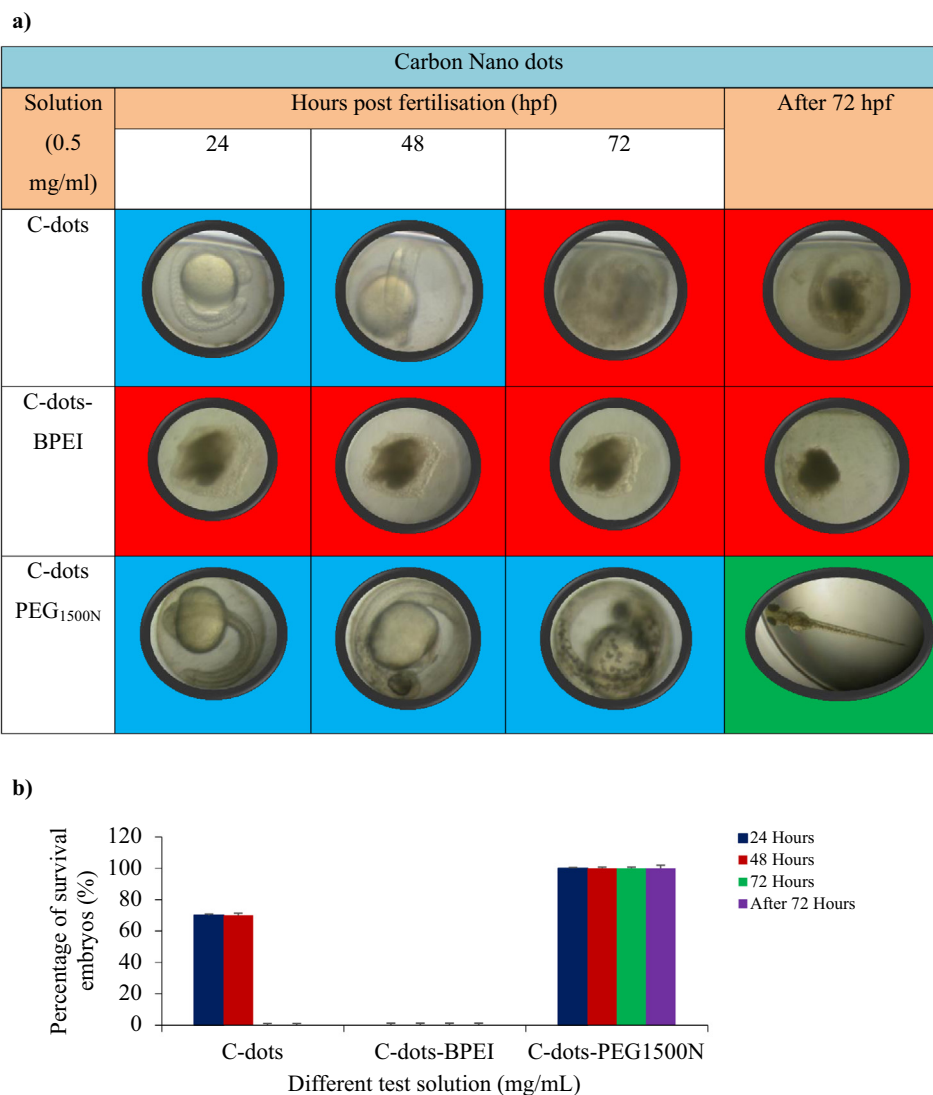


**Fig. 6.** Conditions of zebrafish embryos in different test solutions, (n = 3). (a) Representative images of zebrafish embryos treated with C-dots, C-dots-BPEI and C-dots PEG<sub>1500N</sub>. The red indicated dead embryos, the blue indicated live embryos and the green indicated hatched embryos. (b) Percentage of survival embryos against C-dots, C-dots-BPEI and C-dots PEG<sub>1500N</sub>.

particle. PEG modifies the C-dots flexibility and C-dots can become 'softer' after PEGylation than the underlying material, influencing extravasation (Joker et al., 2011).

Based on these results, it is suggested C-dots modified with PEG<sub>1500N</sub> are suitable for bioimaging, biomedical, or other biological applications mainly due to their non-toxic characteristic to the zebrafish embryos.

#### 4. Conclusions

From this study, the surface modification of C-dots with BPEI and PEG<sub>1500N</sub> using a simple method have been demonstrated. The C-dots passivated with PEG<sub>1500N</sub> were found to be the non-toxic of the modified C-dots tested and, thus, applicable to bioimaging, biomedical, and other related fields. The surface alteration of C-dots with polycations decreased the particle size and they remain within an acceptable range (i.e., <50 nm). This study recommends the modification of C-dots with PEG<sub>1500N</sub> use as a new biomedical nanocarrier with thermal sensing properties. Further study should focus on PEG<sub>1500N</sub>-modified C-dots for the use of a DNA carrier and their applicability in gene therapy.

#### Acknowledgement

This work was financially supported, in part, by research grants DLP-2014-019, FRGS/1/2014/ST01/UKM/03/1, GUP-2014-079, and DIP-2014-016, GUP-2016-014 given by Universiti Kebangsaan Malaysia and the Ministry of Education.

#### Appendix A. Supplementary data

Supplementary data associated with this article can be found, in the online version, at <https://doi.org/10.1016/j.jksus.2018.05.004>.

#### References

- Amjadi, M., Manzoori, J.I., Hallaj, T., Sorouraddin, M.H., 2014. Direct chemiluminescence of carbon dots induced by potassium ferricyanide and its analytical application. *Spectrochim. Acta. A Mol. Biomol. Spectrosc.* 122, 715–720.
- Baker, S.N., Baker, G.A., 2010. Luminescent carbon nanodots: emergent nanolights. *Angew Chem Int Ed.* 49, 6726–6744.
- Bardi, G., Malvindi, M.A., Gherardini, L., Costa, M., Pompa, P.P., Cingolani, R., 2010. The biocompatibility of amino functionalized CdSe/ZnS quantum-dot-doped

- SiO<sub>2</sub> nanoparticles with primary neural cells and their gene carrying performance. *Biomaterials* 31, 6555–6566.
- Bartelmeß, J., Giordani, S., 2014. Carbon nano-onion (multi-layer fullerenes): Chemistry and application. *Beilstein J. Nanotechnol.* 5, 1980–1998.
- Barua, S., Mitra, S., 2014. Challenges associated with penetration of nanoparticles across cell and tissue barriers: A review of current status and future prospects. *Nano Today* 9, 223–243.
- Behnam, B., Shier, W.T., Nia, A.H., Abnous, K., Ramezani, M., 2013. Non-covalent functionalization of single-walled carbon nanotubes with modified polyethyleneimines for efficient gene delivery. *Int. J. Pharm.* 454, 204–215.
- Bianco, A., Kostarelos, K., Prato, M., 2005. Applications of carbon nanotubes in drug delivery. *Curr. Op. Chem. Biol.* 9, 674–679.
- Borse, V., Thakur, M., Sengupta, S., Srivastava, R., 2017. N-doped multi-fluorescent carbon dots for 'turn off-on' silver-biothiol dual sensing and mammalian cell imaging application. *Sens. Act B. Chem.* 248, 481–482.
- Cao, L., Wang, X., Mezziani, M.J., Lu, F.S., Wang, H.F., Luo, P.J.G., 2007. Carbon dots for multiphoton bioimaging. *J. Am. Chem. Soc.* 129, 11318–11319.
- Chen, J.T., Sun, H.Q., Wang, W.L., Xu, W.M., He, Q., Shen, S., Qian, J., Gao, H.L., 2015. Polyethylene glycol modification decreases the cardiac toxicity of carbonaceous dots in mouse and zebrafish models. *Acta Pharm Sinica* 36, 1349–1355.
- Cheng, L., Yang, K., Chen, Q., Liu, Z., 2012. Organic stealth nanoparticles for highly effective in vivo near-infrared photothermal therapy of cancer. *ACS Nano* 6, 5605–5613.
- Chin, S.F., Yazdi, S.N.K.M., Pang, S.C., Ng, S.M., 2012. Facile synthesis of fluorescent carbon nanodots from starch nanoparticles. *Mater. Lett.* 85, 50–52.
- Dong, Y., Shao, J., Chen, C., Li, H., Wang, R., Chi, Y., 2012. Blue luminescent graphene quantum dots and graphene oxide prepared by tuning the carbonization degree of citric acid. *Carbon* 50, 4738–4743.
- Dumortier, H., Lacotte, S., Pastorin, G., Marega, R., Wu, W., Bonifazi, D., 2006. Functionalized carbon nanotubes are non-cytotoxic and preserve the functionality of primary immune cells. *Nano Lett.* 6, 1522–1528.
- Galvez, A., Boime, N.H., Reynaud, C., Clinard, C., Rouzaud, J.N., 2002. Carbon nanoparticles from laser pyrolysis. *Carbon* 40, 2775–2789.
- Gao, H., Pang, Z., Jiang, X., 2013. Targeted delivery of nano-therapeutics for major disorders of the central nervous system. *Pharm Res* 30, 2485–2498.
- Gao, H., Zhang, Q., Yu, Z., He, Q., 2014. Cell-penetrating peptide-based intelligent liposomal systems for enhanced drug delivery. *Curr. Pharm. Biotechnol.* 15, 210–219.
- Hardman, R., 2006. A toxicological review of quantum dots: toxicity depends on physicochemical and environmental factors. *Environ. Health Perspect.* 114, 165–172.
- He, W.T., Xue, Y.N., Peng, N., Liu, W.M., Zhuo, R.X., Huang, S.W., 2011. One-pot preparation of polyethylenimine-silica nanoparticles as serum-resistant gene delivery vectors: intracellular trafficking and transfection. *J. Mater. Chem.* 21, 10496–10503.
- Howe, K.C. et al., 2013. The zebrafish reference genome sequence and its relationship to the human genome. *Nature* 496, 498–503.
- Hsu, P.C., Chang, H.T., 2012. Synthesis of high-quality carbon nanodots from hydrophilic compounds: role of functional group: chemical. *Communication* 48, 3984–3986.
- Huang, P., Lin, J., Li, W., Rong, P., Wang, Z., Wang, S., 2013. Biodegradable gold nanovesicles with an ultrastrong plasmonic coupling effect for photoacoustic imaging and photothermal therapy. *Angew Chem Int Edit.* 52, 13958–13964.
- Huang, Z., Lin, F., Hu, M., Li, C., Xu, T., Chen, C., 2014. Carbon dots with tunable emission, controllable size and their applications for sensing hypochlorous acid. *J. Lumin.* 151, 100–105.
- Jeong, G.S., Lee, S.H., Jeong, S.N., Kim, Y.C., Kim, E.C., 2009. Anti-inflammatory effects of apigenin on nicotine- and lipopolysaccharide-stimulated human periodontal ligament cells via heme oxygenase-1. *Int. Immunopharmacol.* 9, 1374–1380.
- Joker, J.V., Lobovkina, T., Zare, R.N., Gambhir, S.S., 2011. Nanoparticle PEGylation for imaging and therapy. *Nano Med.* 6, 715–728.
- Kam, N.W.S., Jessop, T.C., Wender, P.A., 2004. Nanotube molecular transporters: internalization of carbon nanotube-protein conjugates into mammalian cells. *J. Am. Chem. Soc.* 126, 6850–6851.
- Kettleborough, R.N.W. et al., 2013. A systematic genome-wide analysis of zebrafish protein-coding gene function. *Nature* 496, 494–499.
- Kim, H.Y., Lee, H.J., Kim, J.Y., Lim, W.J., Lim, S.T., 2012. Characterization of nanoparticles prepared by acid hydrolysis of various starch. *Starch* 64, 367–373.
- Kim, H., Namgung, R., Singha, K., Oh, I.I.K., Kim, W.J., 2011. Graphene oxide-polyethylenimine nanoconstruct as a gene delivery vector and bioimaging tool. *Bioconjug Chem.* <https://doi.org/10.1021/bc200397j>.
- Kimmel, C.B., Ballard, W.W., Kimmel, S.R., Ullmann, B., Schilling, T.F., 1995. Stages of embryonic development of the zebrafish. *Dev. Dynam.* 203, 253–310.
- Knop, K., Hoogenboom, R., Fischer, D., Schubert, U.S., 2006. Poly(ethylene glycol) in drug delivery: pros and cons as well as potential alternatives. *Angew Chem. Int. Ed. Engl.* 49, 6288–6308.
- Kumawat, M.K., Thakur, M., Gurung, R.B., Srivastava, R., 2016. Graphene quantum dots from mangifera indica: application in near-infrared bioimaging and intracellular nano-thermometry. *ACS Sustainable Chem. Eng.* <https://doi.org/10.1002/acscschemeng.6b01893>.
- Kuzkova, N., Popenko, O., Yakunov, A., 2014. Application of temperature-dependent fluorescent dyes to the measurement of millimeter wave absorption in water applied to biomedical experiments. *Int. J. Biomed. Imaging.* 2014, 1–5.
- Lee, H., Kim, I.K., Park, T.G., 2010. Intracellular trafficking and unpacking of siRNA/quantum dot-PEI complexes modified with and without cell penetrating peptide: confocal and flow cytometric FRET analysis. *Bioconjug. Chem.* 21, 289–295.
- Lee, C., Kwon, W., Beack, S., Lee, D., Park, Y., Kim, H., Hahn, S.K., Rhee, S., Kim, C., 2016. Biodegradable nitrogen-doped carbon nanodots for non-invasive photoacoustic imaging and photothermal therapy. *Theranostics* 6, 2196–2208.
- Li, H., Kang, Z., Liu, Y., Lee, S.T., 2012. Carbon nanodots: synthesis, properties and applications. *J. Mater. Chem.* 22, 24230–24253.
- Li, Y., Zhong, X., Rider, A.E., Furman, S.A., Ostrikov, K.K., 2014. Fast, energy-efficient synthesis of luminescent carbon quantum dots. *Green Chem.* 16, 2566.
- Lim, S.Y., Shen, W., Gao, Z., 2015. Carbon quantum dots and their application. *Chem. Soc. Rev.* 44, 362–381.
- Liu, M., Chen, B., Huang, J., Zhang, L., Zhang, Z., 2011. Polyamidoamine-grafted multi-walled carbon nanotube for gene delivery: synthesis, transfection and intracellular trafficking. *Bioconjug Chem.* 22, 2237–2243.
- Liu, M., Chen, B., Huang, J., Zhang, L., Zhang, Z., 2011. Polyamidoamine-grafted multiwalled carbon nanotubes for gene delivery: synthesis, transfection and intracellular trafficking. *Bioconjug. Chem.* 22, 2237–2243.
- Liu, S., Tian, J., Wang, L., Zhang, Y., Qin, X., Luo, Y., 2012. Hydrothermal treatment of grass: a low cost, green route to nitrogen-doped, carbon-rich, photoluminescent polymer nanodots as an effective fluorescent sensing platform for label-free detection of Cu(II) ions. *Adv. Mater.* 24, 2037–2041.
- Liu, C., Zhang, P., Zhai, Y., Tian, F., Li, W., Yang, J., Liu, Y., Wang, H., Wang, W., Liu, W., 2012. Nanocarrier for gene delivery and bioimaging based on carbon dots with PEI-passivation enhanced fluorescence. *Biomaterials* 33, 3604–3613.
- Liu, J., Zheng, X., Yan, L., Zhou, L., Tian, G., Yin, W., 2015. Bismuth sulfide nanorods as a precision nanomedicine for in vivo multimodal imaging-guided photothermal therapy of tumor. *ACS Nano* 9, 696–707.
- Mao, X.J., Zheng, H.Z., Long, Y.J., Hao, J.Y., Wang, L.L., Zhou, D.B., 2010. Study on the fluorescence characteristic of carbon dots. *Spec. Act. Part. A.* 75, 553–557.
- Mehta, V.N., Jha, S., Kailasa, S.K., 2014. One-pot green synthesis of carbon dots by using saccharum officinarum juice for fluorescent imaging of bacteria (*Escherichia coli*) and yeast (*Saccharomyces cerevisiae*) cells. *Mater. Sci. Eng. C.* 38, 20–27.
- Mendes, R., Pedrosa, P., Lima, J.C., Fernandes, A.R., Baptista, P.V., 2017. Photothermal enhancement of chemotherapy in breast cancer by visible irradiation of Gold Nanoparticles. *Sci. Rep.* 7, 1–8.
- Menter, J.M., 2006. Temperature dependence of collagen fluorescence. *Photochem. Photobiol. Sci.* 5, 403–410.
- Moghimi, S.M., Andresen, T.C., 2009. Complement-mediated tumor growth: implication for cancer nanotechnology and nanomedicines. *Mol. Immunol.* 46, 1571–1572.
- Namgung, R., Singha, K., Yu, M.K., Jon, S., Kim, Y.S., Ahn, Y., 2010. Hybrid superparamagnetic iron oxide nanoparticle-branched polyethylenimine magnetoplexes for gene transfection of vascular endothelial cells. *Biomaterials* 31, 4204–4213.
- OECD, Draft Proposal for A New Guideline – Fish Embryo Toxicity (FET) Test. Draft Guideline; Organization for Economic Cooperation and Development: Paris, France, 2006.
- OECD, Draft Proposal for A New Guideline – Fish Embryo Toxicity (FET) Test. Draft Guideline; Organization for Economic Cooperation and Development: Paris, France, 2013.
- Oza, G., Oza, K., Pandey, S., Shinde, S., Mewada, A., Thakur, M., Sharon, M., Sharon, M., 2015. A green route towards highly photoluminescent and cytocompatible carbon dots synthesis and its separation using sucrose density gradient centrifugation. *J. Fluoresc.* 25, 9–14.
- Pandey, S., Mewada, A., Oza, G., Thakur, M., Mishra, N., Sharon, M., Sharon, M., 2013. Synthesis and centrifugal separation of fluorescent carbon dots at room temperature. *Nanosci. Nanotechnol.* 5, 775–779.
- Pandey, S., Gedda, G.R., Thakar, M., Wu, H.F., 2017. Theranostic Carbon Dots 'Clathrate-like' nanostructures for targeted photochemotherapy and bioimaging of cancer. *J. Ind. Eng. Chem.* 56, 62–73.
- Pantarotto, D., Briand, J., Prato, M., Bianco, A., 2004a. Translocation of bioactive peptides across cell membranes by carbon nanotubes. *Chem. Commun.* 1, 16–17.
- Pantarotto, D., Singh, R., McCarthy, D., Erhardt, M., Briand, J.P., Prato, M., 2004b. Functionalized carbon nanotubes for plasmid DNA gene delivery. *Angew Chem. Int. Ed.* 43, 5242–5246.
- Papadopoulou, A., Green, R.J., Frazier, R.A., 2005. Interaction of flavonoids with bovine serum albumin: a fluorescence quenching study. *J. Agric. Food Chem.* 53, 158–163.
- Peng, H., Travas-Sejdic, J., 2009. Simple aqueous solution route to luminescent carbonogenic dots from carbohydrates. *Chem. Mater.* 21, 5563–5565.
- Prasad, A.G.D., Kumar, J.K., Sharanappa, P., 2011. Fourier transform infrared spectroscopic study of rare and endanger medical plant. *Rom. J. Biophys.* 21, 221–230.
- Qin, X., Lu, W., Asiri, A.M., Al-Youbi, A.O., Sun, X., 2013. Microwave-assisted rapid green synthesis of photoluminescent carbon nanodots from fluor and their applications for sensitive and selective detection of mercury (II) ion. *Sens. Actuators B Chem.* 184, 156–162.
- Radu, D.R., Lai, C.Y., Jiftinija, K., Rowe, E.W., Jiftinija, S., Lin, V.S., 2004. A polyamidoamine dendrimer-capped mesoporous silica nanosphere-based gene transfection reagent. *J. Am. Chem. Soc.* 126, 13216–13217.
- Ray, S., Saha, A., Jana, R., Sarkar, R., 2009. Fluorescent carbon nanoparticles: synthesis, characterization and bioimaging application. *J. Phys. Chem.* 113, 18546–18551.
- Rubinstein, A.L., 2006. Zebrafish assays for drug toxicity screening. *Expert Opin. Drug Metab. Toxicol.* 2, 231–240.

- Sachdev, A., Gopinath, P., 2015. Green synthesis of multifunctional carbon dots from coriander leaves and their potential application as antioxidants, sensors and bioimaging agents. *Analyst* 140, 4260–4269.
- Sachdev, A., Matai, I., Kumar, S.U., Bhushan, B., Dubey, P., Gopinath, P., 2013. A novel one-step synthesis of PEG-passivated multicolor fluorescent carbon dots for potential biolabeling application. *RSC Adv.* 3, 16958–16961.
- Sha, Y., Lou, J., Bai, S., Wu, D., Liu, B., Ling, Y., 2013. Hydrothermal synthesis of nitrogen-containing carbon nanodots as the high-efficient sensor for copper (II) ion. *Mater. Res. Bull.* 48, 1728–1731.
- Shen, B., Zhang, J., Wu, H., Wang, J., Ma, K., Li, Z., Zhang, X., Zhang, P., Huang, X., 2013. Generation of gene-modified mica via Cos9/RNA-mediated gene targeting. *Cell. Res.* 23, 720–723.
- Sonthanasamy, R.S.A., Ahmad, W.Y.W., Fazry, S., Hassan, N.I., Lazim, A.M., 2015. Transformation of crystalline starch nanoparticles into highly luminescent carbon nanodots: Toxicity studies and their application. *Carbohydr. Polym.* 137, 488–496.
- Sun, Y.P., Zhou, B., Lin, Y., Wang, W., Fernando, K.A.S., Pathak, P., 2006. Quantum-sized carbon dots for bright and colorful photoluminescence. *J. Am. Chem. Soc.* 128, 7756–7757.
- Thakur, M., Pandey, S., Mewada, A., Patil, V., Khade, M., Goshi, E., Sharon, M., 2014. Antibiotic conjugated fluorescent carbon dots as a theranostic agent for controlled drug release, bioimaging and enhanced antimicrobial activity. *J. Drug. Deliv.* 2014, 7794–7809.
- Thakur, M., Mewada, A., Pandey, S., Bhoori, M., Singh, K., Sharon, M., Sharon, M., 2016. Milk-derived multi-fluorescent graphene quantum dot-based cancer theranostic system. *Mat Sci Eng C.* 67, 468–477.
- Thakur, M., Kumawat, M.K., Srivastava, R., 2017. Multifunctional graphene quantum dots for combined photothermal and photodynamic therapy coupled with cancer cell tracking applications. *RSC Adv.* 7, 5251–5261.
- Veiseh, O., Kievit, F.M., Mok, H., Ayesh, J., Clark, C., Fang, C., 2011. Cell transcytosing poly-arginine coated magnetic nanovector for safe and effective siRNA delivery. *Biomaterials* 32, 5717–5725.
- Wang, Y., Hu, A., 2014. Carbon quantum dots. *Synthesis, properties, and application.* *J. Mater. Chem. C.* 2, 6921.
- Wang, Y., Seebald, J.L., Szeto, D.P., Irudayaraj, J., 2010. Biocompatibility and biodistribution of surface-enhanced raman scattering nanoprobe in zebrafish embryos: in vivo and multiplex imaging. *Acs Nano.* 4, 4039–4053.
- Wu, L., Luderer, M., Yang, X., Swain, C., Zhang, H., Nelson, K., 2013. Surface passivation of carbon nanoparticles with branched macromolecules influences near infrared bioimaging. *Theranostics.* 3, 677–686.
- Xu, X.Y., Ray, R., Gu, Y.L., Ploehn, H.J., Gearheart, L., Raker, K., 2004. Electrophoretic analysis and purification of fluorescent single-walled carbon nanotube fragments. *J. Am. Chem. Soc.* 126, 12736–12737.
- Xu, Z., Yu, J., Liu, G., 2013. Fabrication of carbon quantum dots and their application for efficient detecting Ru(bpy)<sub>3</sub><sup>2+</sup> in the solution. *Sens. Actuators B Chem.* 181, 209–214.
- Yan, F., Zou, Y., Wang, M., Mu, X., Yang, N., Chen, L., 2014. Highly photoluminescent carbon dots-based fluorescent chemosensors for sensitive and selective detection of mercury ions and application of imaging in living cells. *Sens. Actuators, B* 192, 488–495.
- Yang, S.T., Cao, L., Luo, P.G., Lu, F., Wang, X., Wang, H., 2009. Carbon dots for optical imaging in vivo. *J. Am. Chem. Soc.* 131, 11308–11309.
- Yang, K., Zhang, S., Zhang, G., Sun, X., Lee, S.T., Liu, Z., 2010. Graphene in mice: ultrahigh in vivo tumor uptake and efficient photothermal therapy. *Nano Lett.* 10, 3318–3323.
- Zhang, P., Liu, W., 2010. ZnO QD@PMAA-co-PDMAEMA nonviral vector for plasmid DNA delivery and bioimaging. *Biomaterials* 31, 3087–3094.
- Zhang, P., Yang, J., Li, W., Wang, W., Liu, C., Griffith, M., 2011. Cationic polymer brush grafted nanodiamond via atom transfer radical polymerization for enhanced gene delivery and bioimaging. *J Mater Chem.* 21, 7755–7764.
- Zhang, J., Yu, S.H., 2016. Carbon dots: large-scale synthesis, sensing and bioimaging. *Mater. Today* 19, 382–393.
- Zhao, Q.L., Zhang, Z.L., Huang, B.H., Peng, J., Zhang, M., Pang, D.W., 2008. Facile preparation of low cytotoxicity fluorescent carbon nanocrystal by electrooxidation of graphite. *Chem. Commun.* 41, 5116–5118.
- Zhou, J., Booker, C., Li, R., Zhou, X., Sham, T.K., Sun, X., 2007. An electrochemical avenue to blue luminescent nanocrystals from multiwalled carbon nanotubes (MWCNTs). *J. Am. Chem. Soc.* 129, 744–745.
- Zhou, X.X., Chung, H.K., Lam, A., Lin, M.Z., 2012. Optical control of protein activity by fluorescent protein domain. *Science* 338, 810–814.
- Zhu, J.H., Li, M.M., Liu, S.P., Liu, Z.F., Li, Y.F., Hu, X.L., 2015. Fluorescent carbon dots for auramine O determination and logic gate operation. *Sens. Actuators B Chem.* 219, 261–267.